J Nanopart Res (2013) 15:2015
DOI 10.1007/s11051-013-2015-5

RESEARCH PAPER

Two-dimensional $Zn_kIn_2O_{k+3}$ nanostructures: synthesis, growth mechanism, self-assembly, and luminescence

Javier Bartolomé · David Maestre · Matteo Amati · Ana Cremades · Javier Piqueras

Received: 25 March 2013 / Accepted: 16 September 2013 / Published online: 27 September 2013

Abstract Indium–zinc oxide nanostructures, such as nanosheets, nanobelts, and wires formed by oriented stacks of nanoplates have been grown by a controlled thermal evaporation method without the use of a foreign catalyst. Surface features in the stacked hexagonal nanoplates suggest a dislocation-driven growth mechanism for these structures. A growth model for these stacks is proposed based on changes in velocity growth rate between the outer and the inner part of the plates. Zn incorporation has been investigated by means of energy-dispersive spectroscopy, X-ray photoelectron spectroscopy, and selected area electron diffraction. The formation of $Zn_kIn_2O_{k+3}$ ternary compounds has been demonstrated. Cathodoluminescence emission and its correlation with the morphology of the structures and Zn content have been studied.

Keywords Indium–zinc oxide · Nanosheets · Transparent conducting oxides · Luminescence and surface electronic properties · Semiconductornanostructure

J. Bartolomé (✉) · D. Maestre · A. Cremades · J. Piqueras
Departamento de Física de Materiales, Universidad Complutense de Madrid, 28040 Madrid, Spain
e-mail: j.bartolome@fis.ucm.es

M. Amati
Sincrotrone Trieste, Area Science Park, 34012 Basovizza-Trieste, Italy

Introduction

Doping of semiconductor nanostructures aimed to modify their physical properties is an active field of research and In_2O_3 nanowires and other nanostructures doped with different elements have been reported. In particular, Sn and Zn doping of In_2O_3 present a high interest related to the applications of indium–tin oxide (ITO) and indium–zinc oxide (IZO) compounds as transparent conductors, field emitters, or as luminescent material. IZO crystalline compounds present a wide range of M ratios [defined as Zn/(Zn + In) atomic ratios] and among them the homologous phases $Zn_kIn_2O_{k+3}$ have been reported. Zn-doped In_2O_3 nanowires have been grown by a vapor–liquid–solid method with the use of a catalyst (Hsin et al. 2006; Zhang et al. 2008; Singh et al. 2010), and Zn-doped microrods have been grown (Bartolomé et al. 2013) by a catalyst-free vapor–solid (VS) method. The same catalyst-free method has been previously used to grow In_2O_3 microrods, as well as In-doped ZnO nanoplates (Alemán et al. 2010), $Zn_kIn_2O_{k+3}$ nanobelts (Alemán et al. 2009), and IZO micropyramids (Bartolomé et al. 2011).

Nanosheets and nanoplates have been previously reported for pure In_2O_3 (Yang et al. 2008) or ZnO (Hosono et al. 2005), as well as for a range of other compound materials (Coleman et al. 2011) and graphene (Geim 2009). They provide improved sensitivity in gas sensor devices (Li et al. 2010), as well as phonon (Mandal et al. 2012) and optical confinement

(Wang et al. 2009). Besides, the dislocation-driven growth of nanorods or nanowires is a timely topic that has been discussed for a limited number of materials (Bierman et al. 2008; Morin et al. 2010a, b; Maestre et al. 2011a) and recently extended to the growth of nanoplates (Morin et al. 2011).

In this work, a mixture of In_2S_3 and ZnO is used as precursor to grow two-dimensional IZO nano- and micro-structures. The mechanism is thermal decomposition of the precursors and subsequent oxidation with formation of indium–zinc oxide structures during the evaporation–deposition process. The introduction of In_2S_3 powders in the precursor causes the growth of IZO different structures by self-assembly of nanosheets. The use of other precursors such as a mixture of InN and ZnO (Bartolomé et al. 2011, 2013) does not lead to the bidimensional growth of plate-like structures.

The structural and optical properties of the structures have been characterized by X-ray diffraction (XRD), transmission electron microscopy (TEM), scanning electron microscopy (SEM), energy-dispersive X-ray spectroscopy (EDS), cathodoluminescence (CL) in SEM and X-ray photoelectron spectroscopy (XPS) carried out at the ESCA beamline in the Elettra Syncrotron (Trieste). The growth mechanism of the structures is discussed and the influence of zinc incorporation on the morphology, luminescence, and surface electronic properties of the structures has been investigated.

Experimental section

The starting material used was a mixture of 5 wt% ZnO (99.9 % purity) and 95 wt% In_2S_3 (99.9 % purity) red powder. The mixture was milled in a centrifugal ball mill in order to homogenize it and was then compacted under load to form a pellet of 7 mm diameter and about 2 mm thickness which was then annealed under argon flow during 10 h at 1,000 or 1,100 °C. During this treatment In_2S_3 decomposes to generate In and S gases (Shen et al. 2005) and since the furnace has not been sealed for vacuum conditions slow formation of indium–zinc oxide compounds takes place resulting in the growth of IZO micro- and nano-structures on the pellet surface. In this process, the ceramic pellet acts as source and simultaneously as substrate for the growth of the micro- and nano-structures at its surface. Since no catalyst or foreign substrate is involved, it is suggested that the formation of the structures takes place by a VS process. For TEM measurements, the structures have been scratched from the surface of the pellets and were then dissolved in toluene and ultrasonicated in order to separate the nanosheets.

XRD measurements were performed in an X′Pert PRO-MRD diffractometer in grazing incidence. The secondary electron and CL observations were carried out in a Leica 440 SEM, a Hitachi S2500 SEM, and a Fei Inspect SEM (the later only in the secondary electron mode). The CL measurements were carried out at room temperature with a beam energy of 15 kV, with a Hamamatsu R928 photomultiplier and a Hamamatsu PMA-11 charge-coupled device camera. TEM images and the corresponding selected area diffraction (SAED) patterns have been recorded in a JEOL JEM 2100 TEM at 200 kV. Local X-ray microanalysis of the structures was performed by EDS with a Bruker AXS 4010 detector in a Leica 440 SEM operating at 15 kV and with an Oxford Inca detector coupled in a JEOL JEM 2100 TEM and a JEOL JEM 2000FX TEM at 200 kV. XPS measurements with spatial resolution in the submicrometer range were carried out in the ESCA microscopy beamline of Elettra Synchrotron facilities, using a 640 eV photon energy with a resolution of 0.2 eV. The scanning photoelectron microscope can work in both spectroscopy and imaging modes, with a zone plate focusing optics that allows using a microprobe with diameter of 150 nm. Therefore, local XPS measurements can be obtained on individual nanostructures.

Results and discussion

After the thermal treatment, the pellet surface contains structures with a marked bidimensional character as nanobelts, nanorings, stacked hexagonal nanoplates, arrays of nanosheets forming nanowalls, and microwire networks containing nanoplates.

XRD spectra of the samples can be assigned to the indium oxide cubic structure with a lattice parameter of 10.12 Å. Neither diffraction peaks of In_2S_3 or ZnO, nor diffraction peaks of IZO have been observed (Fig. 1). Although a part of the grown micro- and nano-structures belong to the series of ternary compounds as described below, the XRD pattern recorded

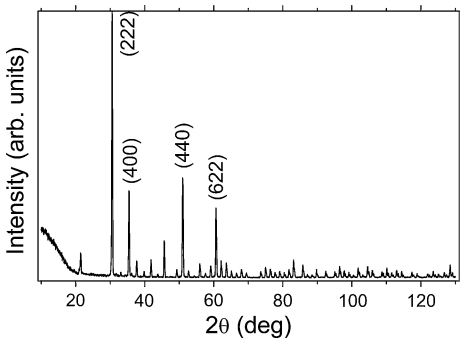

Fig. 1 XRD pattern recorded at grazing incidence

under grazing incidence corresponds to an extended area of the pellet as compared with the size of the structures and hence the XRD signal arises mainly from the pellet.

Figure 2 shows a region containing nanobelts and nanorings. Local EDS spectra show that the value of the In/Zn ratio in the belts is about 0.29 which matches approximately with the composition of a compound of the series $Zn_kIn_2O_{k+3}$ with a k value of 6 or 7. Similar belts and rings have been previously grown by using a precursor mixture of $ZnO–In_2O_3$ containing only 1.4 at% In, and were identified as the $Zn_4In_2O_7$ compound (Alemán et al. 2009). This shows that the $Zn_kIn_2O_{3+k}$ compounds are a rather energetically stable phase during the evaporation–deposition synthesis of IZO compounds, which is obtained with completely different mixtures of compounds as ZnO with few at% of In and In_2S_3 with few at% of Zn.

The plates appear either in form of stacks of hexagonal nanoplates, as structures of connected microwalls or as components of micro- and nano-wire networks. Figure 3a shows the upper hexagonal plate of a stack, with a geometrical distribution of surface growth steps in helical form which suggests the presence of a screw dislocation possibly involved in the growth mechanism. Dislocation-driven growth of nanowires, nanorods, or nanotubes has been demonstrated in the last years for a number of materials, such as PbSe (Zhu et al. 2008), PbS (Bierman et al. 2008), ZnO (Morin et al. 2010a; Alemán et al. 2011), Cu (Meng and Jin 2011), GaN (Cherns et al. 2008), or In_2O_3 (Maestre et al. 2011a, b). Also, the dislocation-driven growth of two-dimensional nanoplates of zinc hydroxy sulfate (ZHS) and Co and Ni hydroxides has been demonstrated by Morin et al. (2011). The hexagonal ZHS plates contained helical steps at the surface showing the presence of dislocations. The helical steps in the nanoplates of this work suggest a dislocation growth mechanism as that described by Morin et al. However, since in the present case the nanoplates form stacks, the growth mechanism should be more complex than that of a single nanoplate. Morin et al. (2011) explained the two-dimensional dislocation-driven growth by a comparable growth rate of steps at the dislocation core and at the outer edge of the plate. On the contrary, if the growth rate at the core steps is higher than that at outer regions, possibly because there are impurity pinning points or slower transport kinetics, the growth of 1D structures is favored. If we consider that the relative growth rates, in the nanoplate plane and in the perpendicular direction can change during the growth due to different adsorption rates at the steps or to variations of transport kinetics during growth, the growth can alternate in the course of time between two-dimension and one-dimension. The result would be stacks of nanoplates joined by a central axis. This model is sketched in Fig. 3e. The corresponding EDS mapping (Fig. 3b) shows a higher In content at the edges of the plates than in the nanoplate front surface. Typical values of In/Zn ratio are about 1 at the edges and about 0.4 on the nanoplate surface. Side view of a stack (Fig. 3c) shows that the thickness of the nanoplates is between 100 and 300 nm. Representative CL spectrum of the nanoplates is shown in Fig. 3d in comparison with the undoped In_2O_3. Typically, the undoped In_2O_3 CL emission consists of a single broadband centered at 1.9 eV which has been described in several works for both indium oxide polycrystalline thin films (Lee et al. 1996) and

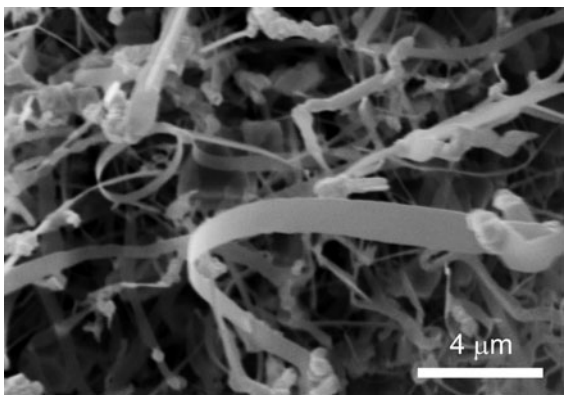

Fig. 2 SEM image of nanobelts and nanorings

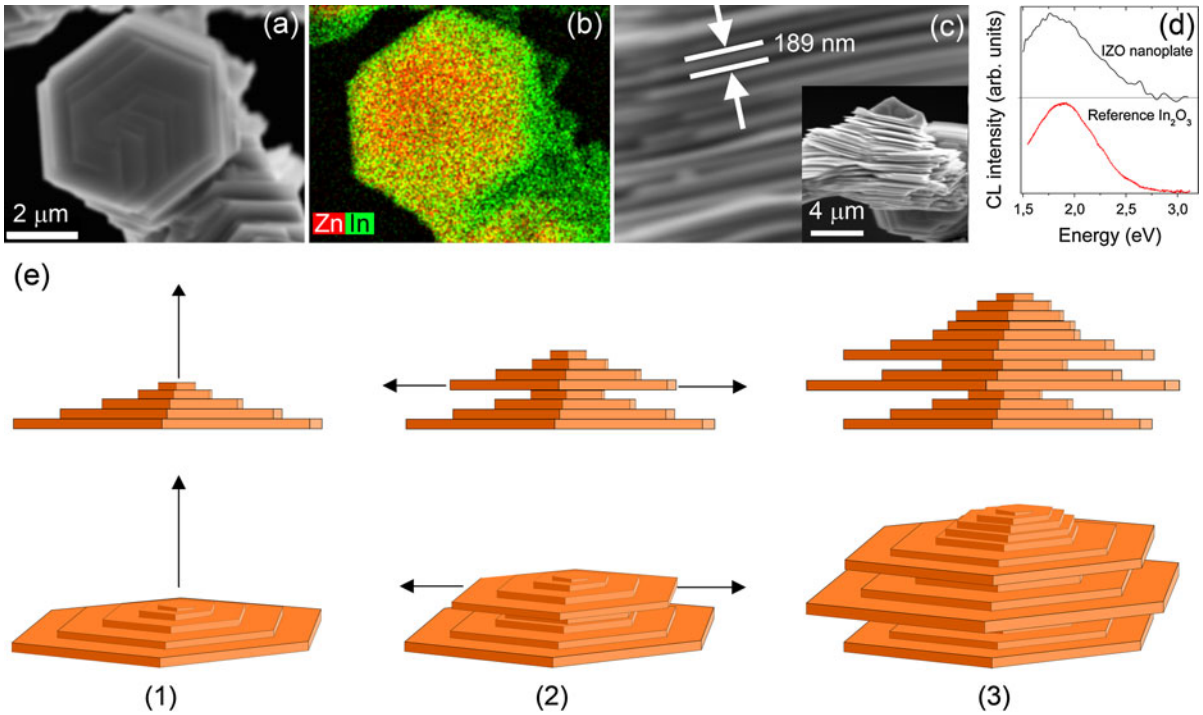

Fig. 3 **a** SEM image of a *hexagonal plate* with steps in its surface. **b** Corresponding EDS mapping. **c** Side view of a stack of nanoplates showing a typical thickness of few hundreds of nanometers. *Inset* shows a less magnified image of the stack. **d** Corresponding CL spectrum compared with reference In_2O_3 spectrum. **e** Growth model sketch of *hexagonal nanoplates* stacks: the change in the growing velocity rate between the steps near the core and at the edges of the plates causes the alteration between one-dimensional (*1*) and two-dimensional (*2*) growth of the top-most part of the structure. Repetition of these velocity rate changes during the treatment leads to the observed structures (*3*)

nanostructures (Magdas et al. 2006; Jeong et al. 2004; Mazzera et al. 2007). This orange band has been frequently attributed to oxygen vacancies but its exact origin remains unknown. Emission in the 2.2–2.6 eV range is also observed in undoped nanostructures and has been attributed to oxygen vacancies (Zheng et al. 2001; Tang et al. 2005; Guha et al. 2004). CL spectra of the nanoplates (Fig. 3d) show a broad orange band with a low contribution in the range of 2.2–2.6 eV. The peak maximum is shifted from 1.9 to 1.8 eV, and the total CL intensity seems to be considerably reduced with respect to the emission of the In_2O_3 substrate. Although both spectra are rather similar, the high Zn content measured by EDS in the plates and the XPS results that will be described below suggest that the origin of the emission in the plates should be attributed not to an In_2O_3 emission modified by Zn doping, but to an IZO characteristic band.

Figures 4a, b show the SEM secondary electron image and the ratio between In ($3d_{5/2}$) and Zn ($3d$) core-level signal-based image of one hexagonal plate. Higher content of In is found not only in the edges of the plate, in agreement with the EDS results, but also in the edge of the steps, where EDS mapping shows no features. These composition changes along the nanoplate surface could contribute to the mentioned growth rates changes in different surface steps. XPS spectra obtained from different points of the plates show almost no variation in shape or position of the In ($3d$) (Fig. 4c), in agreement with the previously reported values for In^{3+} cation (Fan and Goodenough 1977). The Zn ($3d$) peak is centered at 9.57 eV (Fig. 4d), shifted from the reference Zn ($3d$) core level for ZnO (Gaarenstroom and Winograd 1977; Ley et al. 1974). This shift can be interpreted as an evidence of the formation of IZO homologous series compounds (Bartolomé et al. 2013); (Kumar et al. 2005). The value from valence-band edge (VBE) to the Fermi level measured from the valence-band onset is different in points with different amounts of Zn. As shown in

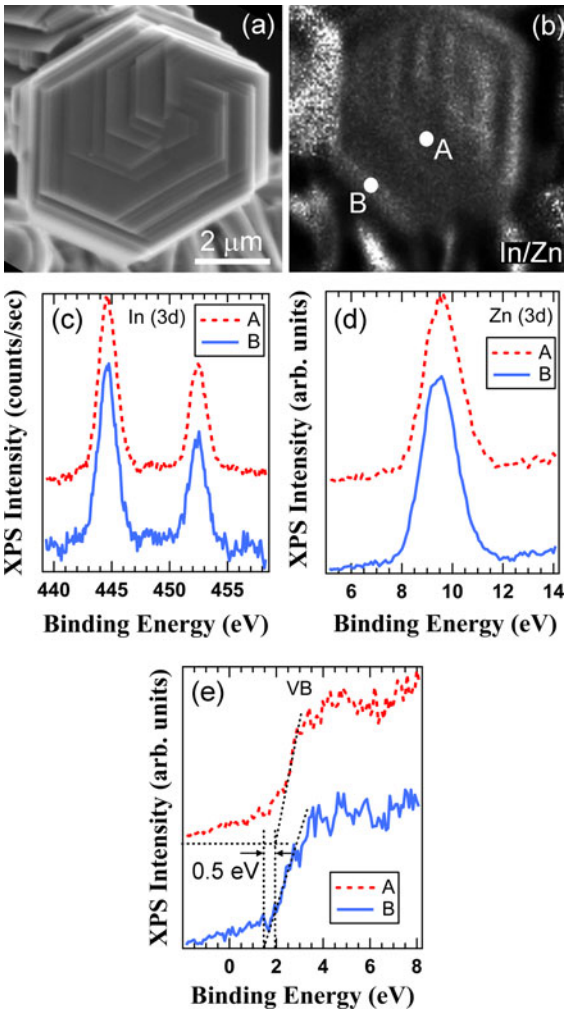

Fig. 4 **a** SEM image of a hexagonal plate. **b** Corresponding XPS signal-based image. The ratio of In (3*d*) and Zn (3*d*) signals has been represented in order to avoid topography effects. **c**–**e** Comparison of the In (3*d*), Zn (3*d*), and valence-band spectra, respectively, measured at points indicated in (**b**)

Fig. 4e, the VBE is shifted toward lower BE from 1.4 eV at the edge of the plate, where less Zn is found, to 1.9 eV in regions with more Zn concentration in agreement with a more pronounced *n*-type behavior when more Zn is introduced in the ternary composition (Bartolomé et al. 2013).

Other arrangement of the plates is a structure of microwalls which either covers a large area of the sample (Fig. 5a) or form aggregates (Fig. 5b) dispersed on the pellet surface. The Zn content in the walled structures was found to vary in a large range; in particular, the In/Zn ratio in the aggregate of Fig. 5b was about 0.45. Growth of micro- and nano-walled

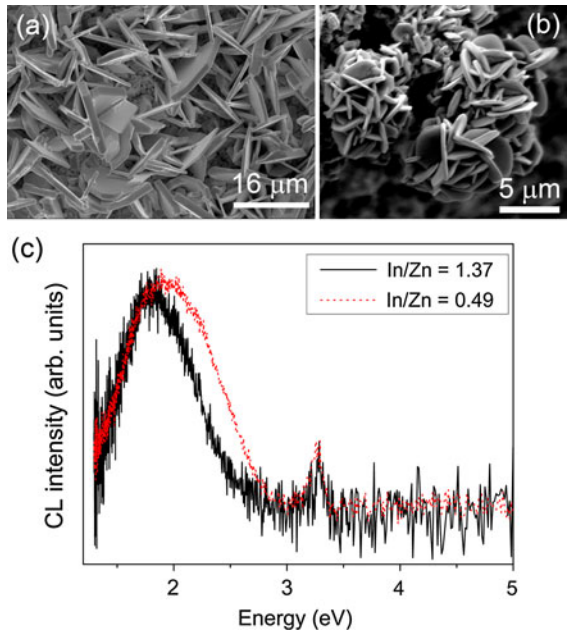

Fig. 5 **a** SEM image of a large substrate area covered with plates. **b** SEM image of an aggregate of microplates. **c** CL spectra of two regions of microplates with different In/Zn ratios

structures, with a high surface to volume ratio, is of potential interest in fields such as photocatalysis, sensing, or field emission. ZnO nanowalls have been previously grown by a vapor–liquid–solid process with gold as catalyst (Lao et al. 2004; Ng et al. 2003), and by electrodeposition (Pradhan et al. 2008). Alemán et al. (2010) grew indium-doped ZnO nanowalls by the same catalyst free evaporation–deposition method used here, with a mixture of ZnS and In_2O_3 as precursor, while the mixture ZnO–In_2O_3 does not lead to the formation of micro- or nano-walls as found in this work and by Yan et al. (2008). The present results show how the precursor used determines to a large extent the final morphology of the obtained indium–zinc oxide nanostructures. CL spectra of these regions also present a widening of the 1.9 eV band for lower In/Zn ratio, as already reported for the hexagonal stacks of nanoplates, but as a difference a weak band at 3.2 eV associated to the band gap emission is recorded at the walls (Fig. 5c). The detection of a band gap luminescence should be related to the presence of IZO phase in these samples, as the band gap of indium oxide is usually absent in luminescence measurements due to dipole forbidden character of the transitions between the highest valence-band states and states at the conduction-band minimum (King et al. 2009).

Nanoplates are also present in branched microwire structures, which form dense networks of nano- and micro-wires. The building block of the network is a structure composed of a main wire on which the secondary growth develops as shown in Fig. 6a. The network is formed by interconnected wires covering large areas of the pellet as shown in Fig. 6b. The branches are formed by stacks of nanoplates (Fig. 6c) with typical In/Zn ratios around 0.50 as measured by EDS. Some small plates could be separated by scratching the sample containing the networks, as described in the experimental section, and were observed in TEM to perform EDS and SAED analysis. Figure 6d shows the TEM image of one of these plates. SAED and EDS measurements (inset in Fig. 6d, e) correspond to a ternary oxide with $k = 7$ for this structure, although a wide range of values, corresponding to different ternary oxides has been obtained. The presence of Zn is also detected by an increase of the total CL signal and by the enhancement of the emission bands at 2.35 eV, as shown in Fig. 6f. A narrow band centered at 2.37 eV has been described to be characteristic of the IZO ternary compound $Zn_4In_2O_7$ (Alemán et al. 2009), while a broadening of the 1.9 eV characteristic band toward higher energies has been described for two different Sn-doped IZO with the general chemical formula of $Sn:Zn_kIn_2O_{k+3}$ ($k = 4$ and 5) (Na et al. 2005). Hence, the presence of an emission band centered at 2.35 eV in our samples points out to the formation of ternary compounds of

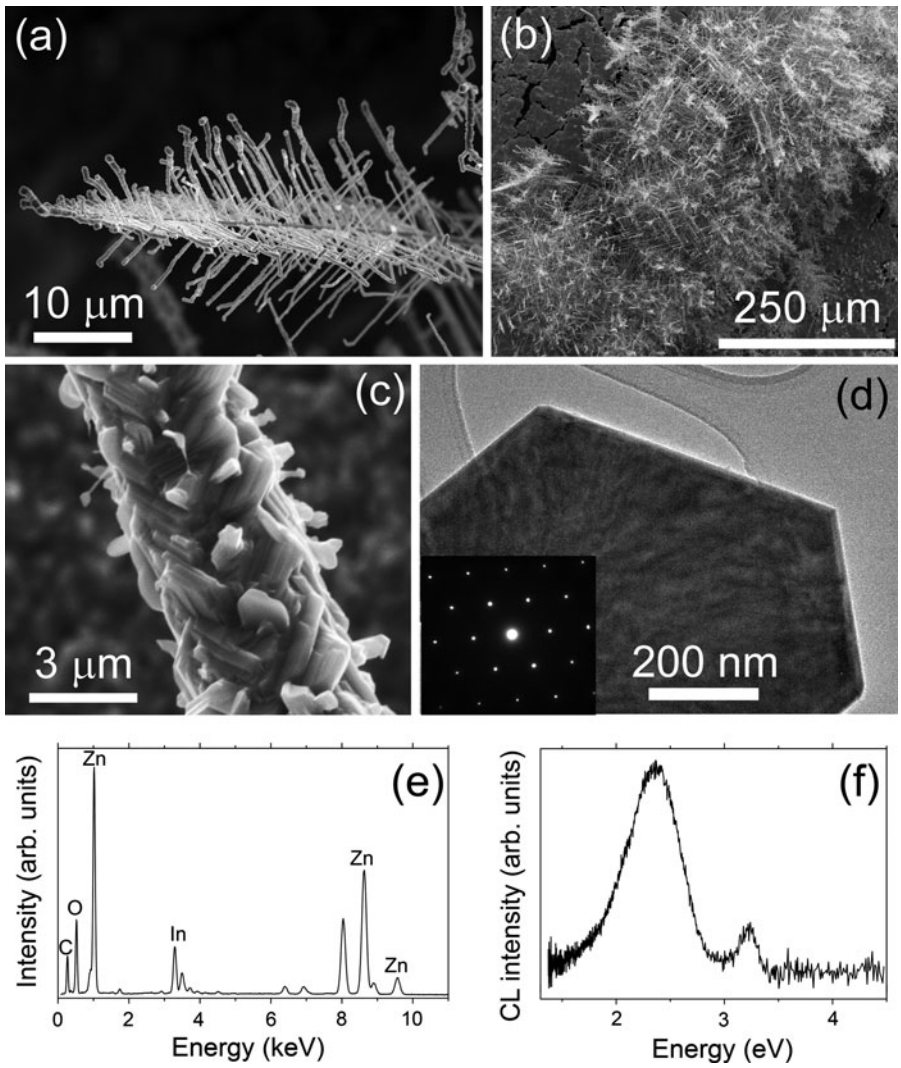

Fig. 6 **a** SEM image of one branched structure composed by a main wire and secondary grown nanowires. **b** SEM image showing a large area covered by branched and networked structures. **c** Detail of one microwire composed by stacked nanoplates. **d** TEM image of one separated nanoplate. *Inset* shows the corresponding SAED pattern. **e** EDS pattern from the plate shown in (**d**). Additional peaks (not labeled) come from the sample holder grid. **f** CL spectrum recorded from free-standing branched micro- and nano-structures

the homologous series of $Zn_kIn_2O_{k+3}$, which agrees with the Zn/In ratio measured by EDS.

Conclusions

In summary, indium–zinc oxide nanoplates have been grown by a catalyst-free method. Using a mixture of In_2S_3 and ZnO powders as precursor, the bidimensional growth of nanostructures is enhanced over the one-dimensional growth previously obtained with InN and ZnO precursors. XPS, SAED, and CL results demonstrate that these structures are formed by ternary compounds of the $Zn_kIn_2O_{k+3}$ family with a broad range of k values. Changes in their morphology and Zn content lead to different luminescence properties. For stacked plates or connected microwalls a broadening of the characteristic 1.9 eV band is observed for decreasing In/Zn ratio, while for nanosheets forming micro- and nano-wires by self-assembly a new emission at 2.35 eV related to the presence of IZO compounds as well as quenching of the characteristic 1.9 eV band is observed. Helical surface steps in hexagonal nanoplates indicate the existence of a dislocation-driven growth mechanism. It is suggested that the formation of stacks of nanoplates is related to variations of deposition rates during growth.

Acknowledgments This work has been supported by Ministerio de Economía y Competitividad (Projects MAT 2012-31959, and Consolider CSD 2009-00013). J. Bartolomé acknowledges the financial support from Universidad Complutense de Madrid.

References

Alemán B, Fernández P, Piqueras J (2009) Indium-zinc-oxide nanobelts with superlattice structure. Appl Phys Lett 95:013111

Alemán B, Fernández P, Piqueras J (2010) Dense vertical nanoplates arrays and nanobelts of indium doped ZnO grown by thermal treatment of ZnS–In_2O_3 powders. J Cryst Growth 312:3117–3120

Alemán B, Ortega Y, García JA, Fernández P, Piqueras J (2011) Fe solubility, growth mechanism, and luminescence of Fe doped ZnO nanowires and nanorods grown by evaporation–deposition. J Appl Phys 110:014317

Bartolomé J, Maestre D, Cremades A, Amati M, Piqueras J (2011) Indium zinc oxide pyramids with pinholes and nanopipes. J Phys Chem C 115:8354–8360

Bartolomé J, Maestre D, Cremades A, Amati M, Piqueras J (2013) Composition-dependent electronic properties of indium–zinc–oxide elongated microstructures. Acta Mater 61:1932–1943

Bierman MJ, Lau YKA, Kvit AV, Schmitt AL, Jin S (2008) Dislocation-driven nanowire growth and Eshelby twist. Science 320:1060–1063

Cherns D, Meshi L, Griffiths I, Khongphetsak S, Novokov SV, Farley NRS, Campion RP, Foxon CT (2008) Defect-controlled growth of GaN nanorods on (0001)sapphire by molecular beam epitaxy. Appl Phys Lett 93:111911

Coleman JN, Lotya M, O'Neill A, Bergin SD, King PJ, Khan U, Young K, Gaucher A, De S, Smith RJ et al (2011) Two-dimensional nanosheets produced by liquid exfoliation of layered materials. Science 331:568–571

Fan JCC, Goodenough JB (1977) X-ray photoemission spectroscopy studies of Sn-doped indium-oxide films. J Appl Phys 48:3524–3531

Gaarenstroom SW, Winograd N (1977) Initial and final state effects in the ESCA spectra of cadmium and silver oxides. J Chem Phys 67:3500–3506

Geim AK (2009) Graphene: status and prospects. Science 324:1530–1534

Guha P, Kar S, Chaudhuri S (2004) Direct synthesis of single crystalline In_2O_3 nanopyramids and nanocolumns and their photoluminescence properties. Appl Phys Lett 85: 3851–3853

Hosono E, Fujihara S, Honma I, Zhou H (2005) The fabrication of an upright-standing zinc oxide nanosheet for use in dye-sensitized solar cells. Adv Mater 17:2091–2094

Hsin CL, He JH, Chen LJ (2006) Modulation of photoemission spectra of In_2O_3 nanowires by the variation in Zn doping level. Appl Phys Lett 88:063111

Jeong JS, Lee JY, Lee CJ, An SJ, Yi G-C (2004) Synthesis and characterization of high-quality In_2O_3 nanobelts via catalyst-free growth using a simple physical vapor deposition at low temperature. Chem Phys Lett 384:246–250

King PDC, Veal TD, Fuchs F, Wang CY, Payne DJ, Bourlange A, Zhang H, Bell GR, Cimalla V, Ambacher O et al (2009) Band gap, electronic structure, and surface electron accumulation of cubic and rhombohedral In_2O_3. Phys Rev B 79:205211

Kumar B, Gong H, Akkipeddi R (2005) A study of conduction in the transition zone between homologous and ZnO-rich regions in the In_2O_3–ZnO system. J Appl Phys 97:063706

Lao JY, Huang JY, Wang DZ, Ren ZF, Steeves D, Kimball B, Porter W (2004) ZnO nanowalls. Appl Phys A 78:539–542

Lee MS, Choi WC, Kim EK, Kim CK, Min SK (1996) Characterization of the oxidized indium thin films with thermal oxidation. Thin Solid Films 279:1–3

Ley L, Pollak RA, McFeely FR, Kowalczyk SP, Shirley DA (1974) Total valence-band densities of states of III–V and II–VI compounds from X-ray photoemission spectroscopy. Phys Rev B 9:600–621

Li J, Fan H, Jia X (2010) Multilayered ZnO nanosheets with 3D porous architectures: synthesis and gas sensing application. J Phys Chem C 114:14684–14691

Maestre D, Häussler D, Cremades A, Jäger W, Piqueras J (2011a) Nanopipes in In_2O_3 nanorods grown by a thermal treatment. Cryst Growth Des 11:1117–1121

Maestre D, Häussler D, Cremades A, Jäger W, Piqueras J (2011b) Complex defect structure in the core of Sn-Doped In_2O_3 nanorods and its relationship with a dislocation-

driven growth mechanism. J Phys Chem C 115: 18083–18087

Magdas DA, Cremades A, Piqueras J (2006) Growth and luminescence of elongated In_2O_3 micro- and nanostructures in thermally treated InN. Appl Phys Lett 88:113107

Mandal A, Mitra S, Datta A, Banerjee S, Dhara S, Chakravorty D (2012) Multiphonon scattering and photoluminescence of two dimensional ZnS nanosheets grown within Na-4 mica. J Appl Phys 112:074321

Mazzera M, Zha M, Calestani D, Zappettini A, Lazzarini L, Salviati G, Zanotti L (2007) Low-temperature In_2O_3 nanowire luminescence properties as a function of oxidizing thermal treatments. Nanotechnology 18:355707

Meng F, Jin S (2011) The solution growth of copper nanowires and nanotubes is driven by screw dislocations. Nano Lett 12:234–239

Morin SA, Jin S (2010) Screw dislocation-driven epitaxial solution growth of ZnO nanowires seeded by dislocations in GaN substrates. Nano Lett 10:3459–3463

Morin SA, Bierman MJ, Tong J, Jin S (2010) Mechanism and kinetics of spontaneous nanotube growth driven by screw dislocations. Science 328:476–480

Morin SA, Forticaux A, Bierman MJ, Jin S (2011) Screw dislocation-driven growth of two-dimensional nanoplates. Nano Lett 11:4449–4455

Na CW, Bae SY, Park J (2005) Short-period superlattice structure of Sn-doped $In_2O_3(ZnO)_4$ and $In_2O_3(ZnO)_5$ nanowires. J Phys Chem B 109:12785–12790

Ng HT, Li J, Smith MK, Nguyen P, Cassell A, Han J, Meyyappan M (2003) Growth of epitaxial nanowires at the junctions of nanowalls. Science 300:1249

Pradhan D, Kumar M, Ando Y, Leung KT (2008) Efficient field emission from vertically grown planar ZnO nanowalls on an ITO-glass substrate. Nanotechnology 19:035603

Shen G, Bando Y, Lee C-J (2005) Growth of self-organized hierarchical ZnO nanoarchitectures by a simple In/In_2S_3 controlled thermal evaporation process. J Phys Chem B 109:10779–10785

Singh N, Yan C, Lee PS (2010) Room temperature CO gas sensing using Zn-doped In_2O_3 single nanowire field effect transistors. Sens Actuatators B 150:19–24

Tang Q, Zhou W, Zhang W, Ou S, Jiang K, Yu W, Qian Y (2005) Size-controllable growth of single crystal $In(OH)_3$ and In_2O_3 nanocubes. Cryst Growth Des 5:147–150

Wang NW, Yang YH, Yang GW (2009) Indium Oxide–Zinc oxide nanosized heterostructure and whispering gallery mode luminescence emission. J Phys Chem C 113: 15480–15483

Yan Y, Zhou L, Zhang Y, Zhang J, Hu S (2008) Large-scale synthesis of In_2O_3 nanocubes under nondynamic equilibrium model. Cryst Growth Des 8:3285–3289

Yang H, Zhang R, Dong H, Yu J, Yang W, Chen D (2008) In situ growth of self-assembled and single In_2O_3 nanosheets on the surface of indium grains. Cryst Growth Des 8: 3154–3159

Zhang W, Jie J, He Z, Tao S, Fan X, Zhou Y, Yuan G, Luo L, Zhang W, Lee CS et al (2008) Single zinc-doped indium oxide nanowire as driving transistor for organic light-emitting diode. Appl Phys Lett 92:153312

Zheng MJ, Zhang LD, Li GH, Zhang XY, Wang XF (2001) Ordered indium-oxide nanowire arrays and their photoluminescence properties. Appl Phys Lett 79:839–841

Zhu J, Peng H, Marshal AF, Barnett DM, Nix WD, Cui Y (2008) Formation of chiral branched nanowires by the Eshelby twist. Nat Nanotechnol 3:477–481